A 3D Optical Metamaterial Made by Self-Assembly

Silvia Vignolini, Nataliya A. Yufa, Pedro S. Cunha, Stefan Guldin, Ilia Rushkin, Morgan Stefik, Kahyun Hur, Ulrich Wiesner, Jeremy J. Baumberg, and Ullrich Steiner**

The prediction and subsequent creation of artificially engineered metamaterials has opened the pathway to revolutionary effects in light–matter interactions.[1–6] In such materials the properties of the dielectric and magnetic permittivities, ε and μ, are not governed by the response of the individual atoms in the presence of an electromagnetic field, but are determined by the sub-wavelength structure of the material. In 1996 Pendry et al. predicted that a sparse cubic metal wire array with micrometer-wide wires would have a significantly reduced plasma frequency due to the reduced average electron density and the large self-inductance of the structure.[2]

A plethora of experimental work in this field has demonstrated metamaterials from GHz[7] up to yellow optical frequencies.[8] Reaching higher optical frequencies has proven problematic, as it requires the manipulation of materials on the scale of just a few tens of nanometers over macroscopic areas. While fabrication techniques such as focused ion beam lithography, direct laser writing, and atomic layer deposition[9–13] provide design flexibility, they are limited with regard to accessible feature sizes as well as the scalability of samples.

Until now, colloidal self-organization was the only type of self-assembly used to create metamaterials.[14] These materials have feature sizes limited to above several hundreds of nanometers and to sphere-packing geometries. Block copolymers (BCPs) are unique in offering a route to creating macroscopically large samples with a variety of complex 3D architectures with features on the nanometer length scale. Unlike earlier work based on BCPs,[15] we incorporate a continuous metal phase into a BCP scaffold,[16] thereby producing the first truly optical, 3D metamaterial. As predicted by Pendry et al.,[2] this material has a reduced plasmon frequency. In addition, it exhibits strongly anisotropic plasmon modes with linear dichroism and optical chirality across the visible region.

Dr. S. Vignolini, Dr. N. A. Yufa, P. S. Cunha, S. Guldin,
Prof. J. J. Baumberg, Prof. U. Steiner
Cavendish Laboratory
Department of Physics
University of Cambridge
J. J. Thomson Avenue
Cambridge CB3 0HE, UK
E-mail: jjb12@cam.ac.uk; u.steiner@phy.cam.ac.uk
Dr. I. Rushkin
Department of Mathematics
University of Nottingham
University Park
Nottingham NG7 2RD, UK
Dr. M. Stefik, K. Hur, Prof. U. Wiesner
Department of Materials Science and Engineering
Cornell University, Ithaca, New York 14853, USA

DOI: 10.1002/adma.201103610

BCPs are polymers that consist of two or more distinct polymer chains (blocks) joined by a covalent bond. The interplay between the energetic penalty for stretching the blocks is balanced by the chemical repulsion between the blocks, creating a range of morphologies such as spheres, cylinders, and gyroids.[17] Increasing the number of blocks leads to an increase in the number of accessible morphologies.[18]

There has been previous work using BCP scaffolds with dielectrics for optical applications.[19] In this work, however, we opt to replace one of the continous nanoscale polymer networks with a metal in order to create a novel material with interesting optical properties that are very different from those of a structured dielectric. Such replication is possible because the blocks in BCPs are chemically distinct, hence we can selectively etch them and then backfill with inorganic materials to replicate self-assembled structures into materials that are not amenable to direct self-assembly in such complex morphologies.

Here, we demonstrate the creation of a 3D gold metamaterial based on BCP self-assembly. We start with an isoprene-*block*-styrene-*block*-ethylene oxide (ISO) BCP that forms two chemically distinct, interpenetrating gyroid networks (I,O) of opposite chirality in a matrix of the third block.[20] The I gyroid network is then removed by selective UV and chemical etching and backfilled with gold by electrodeposition. The final device consists of a continuous, triply periodic network of gold (**Figure 1**). The dimension of the full unit cell is ≈50 nm, which is far below optical wavelengths. This particular morphology has been chosen since it is predicted to offer a strong resonant response that depends on the relative orientation between the structure and the polarization of the incident light. Figure 1a shows the [110] projection of the gyroid.

Samples were prepared using ISO BCP films, which are known to self-assemble into the gyroid morphology with a chiral isoprene phase, as is schematically shown in **Figure 2**. We utilized a poly(ISO) prepared by sequential anionic polymerization using standard methods.[18,21] The molecular weight of the polyisoprene block was determined by gel permeation chromatography (GPC); the molecular weights of the polystyrene and poly(ethylene oxide) blocks were determined by NMR, and the final polydispersity was determined by GPC. The ISO used in this study was composed of 14.63, 29.04, and 9.77 kg mol^{-1} of I, S, and O, respectively, with a molecular weight of 53.44 kg mol^{-1} and a polydispersity of 1.05. A detailed characterization of this polymer shows self-assembly into the alternating gyroid phase.[20] Polymer film scaffolds were prepared by blade-coating a 5% w/v ISO anisole solution onto glass substrates with a conducting coating for electrodeposition. The resulting films were exposed to UV light (254 nm) for 3 h and rinsed with ethanol to remove the isoprene. The resulting pore network was backfilled with gold by electrodeposition to a thickness of 200 nm. Thicker

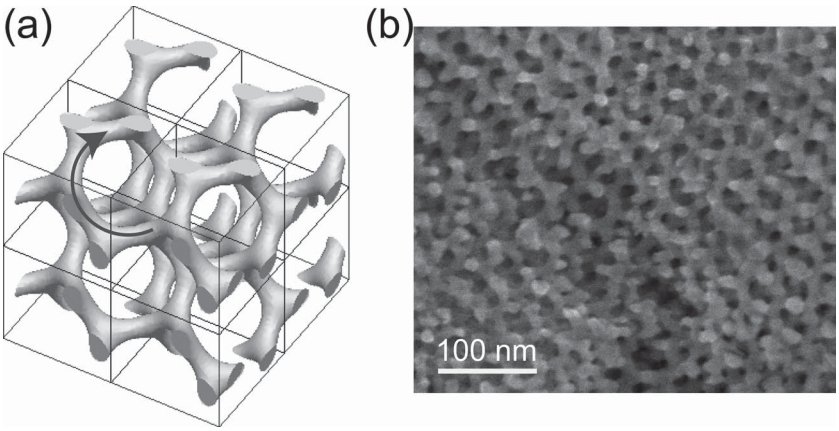

Figure 1. Gyroid morphology. a) A computer-simulated view of the single gyroid. The arrow indicates the handedness along the [111] axis. b) Scanning electron microscopy (SEM) image of a metal gyroid by filling a porous polymer network.

samples were also prepared and will be the subject of a future study. In the electrochemical setup, a saturated calomel electrode was used as the reference. The deposition consisted of a nucleation and a deposition step. The nucleation step consisted of 1 to 3 cyclic voltammetry scans between 0 V and –1.2 V at a scan rate of 50 mV s^{-1}. The deposition step at a fixed potential of –0.8 V for 100 s resulted in a final thickness of about 200 nm. The remaining polymer was removed by plasma etching.

The samples were spectroscopically characterized using a white-light-illuminated optical microscope with fiber detection in a confocal configuration. In **Figure 3** the experimental results for both reflection and transmission configurations with unpolarized incident light are compared with the results of calculation of the ideal structures using a finite difference time domain code[22] employing the material parameters for gold.[23] In the comparison, we have to take into account an ≈5 nm thick solid Au layer at the bottom of the gyroid layer, which is not included in the calculation. The presence of this layer partially reduces the transmission of the fabricated ≈200 nm thick sample. A simple Maxwell–Garnett averaging of the refractive index of the Au/air composite with the same Au fill fraction of $f = 21\%$ predicts near-perfect transmission in the red and infrared, completely opposite to the observation in Figure 3. In fact, the presence of an ordered and continuos nanometer-scale gyroid network results in a reduction of the plasma frequency of gold. This is also confirmed by finite difference time domain calculations. The qualitative agreement between the spectra in Figure 3 show a decrease in reflection at about 600 nm that can be explained in terms of the Drude model in a reduction of plasma frequency from the bulk value of 7.5 eV to 1.55 eV. Thus, the composite gyroid material behaves like a new metal with its own distinct optical characteristics: a plasma edge at 750 nm and a transparency that is greatly increased compared to any naturally occurring bulk metal.

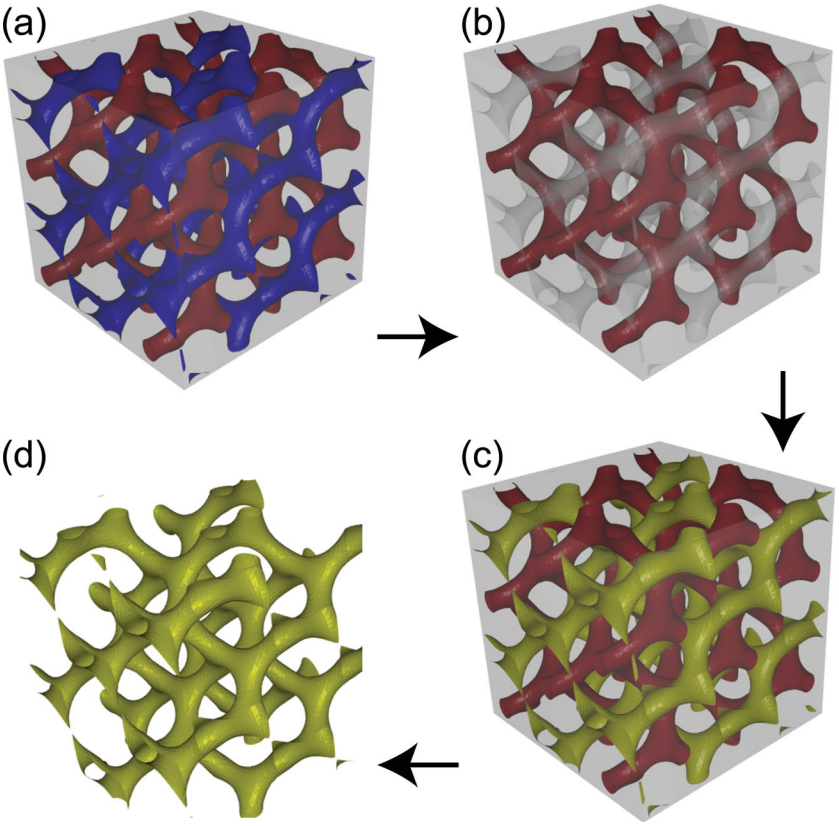

Figure 2. Schematic representation of sample fabrication. a) The three different colors (red, blue, and grey) correspond to the different blocks of the copolymer. The isoprene block (blue) is removed in (b) and is then back-filled with gold (yellow) in (c). The final structure is obtained by plasma etching the two remaining polymer blocks, revealing a 3D continuous gold network in air in (d).

Two contributions are responsible for the modified plasma wavelength, $\lambda_p = \lambda_p^{Au}\, m_{eff}/f$ (where m_{eff} is the effective mass of the electrons in the actual material, f the filling fraction), from that of Au (λ_p^{Au} = 165 nm). The network of Au struts surrounded by air reduces the net electron density and accounts for about half of the reduction in the plasma frequency. The other contribution comes from the increased self-inductance of the structure produced when multiply-connected wires are formed that span all three spatial axes.

The SEM image in **Figure 4**a reveals the morphology of the sample on the length scale of tens of micrometers. While the single gyroid has the same orientation perpendicular to the substrate surface across the entire sample, twinning in lateral directions is found, with domain sizes of 10–100 μm.

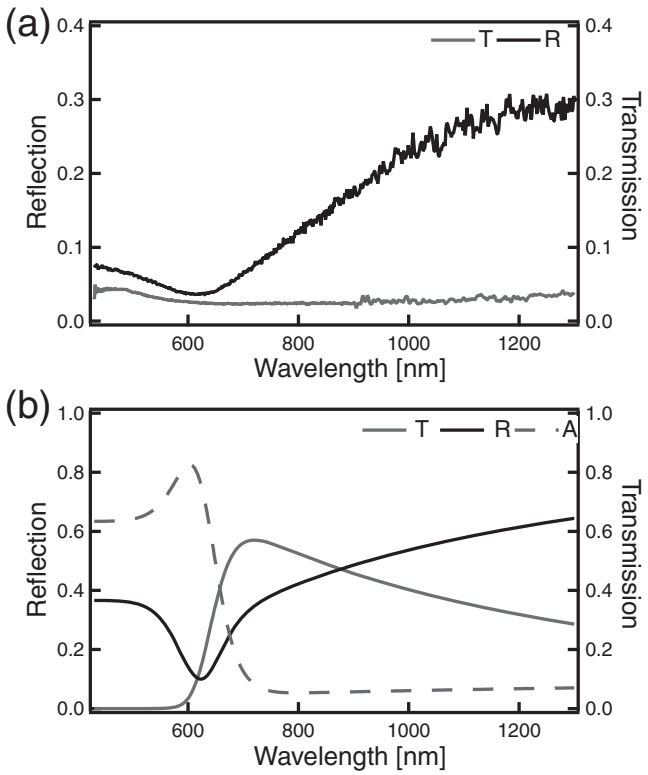

Figure 3. Transmission and reflection spectra for unpolarised incident light. a) Experimental data compared with b) the finite difference time domain calculations of a full 3D representation of the gyroid.

The angle between the [100] direction at the twinning boundary is approximately 105°. Since the structure is anisotropic, its optical response strongly depends on the gyroid orientation. The investigated samples were therefore marked using a micromanipulator, in order to precisely relate the spectroscopic measurements to the twinning morphology obtained by SEM.

Imaging and spectroscopy in reflection under linearly polarized illumination show a clear birefringence across each twinned gyroid domain, observed as strong color changes in Figure 4b,c and Movie S1 (Supporting Information). When the grain boundary is perpendicular to the polarization direction, light is coupled equally into the two twinned domains, which results in identical reflected color (Figure 4b). Since the twinning angle between the two regions is 105°, when the polarization of the incident light is parallel to the [100] direction of one of the areas it is nearly perpendicular to the [100] direction of its twin, resulting in different colors in reflection (Figure 4c, Supporting Information Movie S1). Two different reflection spectra are observed in the orthogonal directions (Figure 4d), with an admixture between them as the polarization direction is varied. These reflection spectra show increasing absorption at shorter wavelengths with a peak that tunes sinusoidally with the polarization direction between 525 and 630 nm, as shown in Figure 4e for one of the domains. In addition to this shift in the absorption peak position, the spectral linewidth of the absorption band is a function of the polarization direction and tracks the observed spectral shifts. Performing the same analysis for the twin domain reveals a spectral modulation with the same period and amplitude but with a phase shift that is in perfect agreement with the twinning angle between the domains.

Light polarized in different directions couples differently to localized plasmon resonances of the interconnected gold network. A simple way to understand this behavior is to approximate the gyroid as a network of disconnected Au rods. In the gyroid sample, a short-wavelength resonance is seen for a polarization along the [100] direction of the domain, which is red-shifted by 20% in the perpendicular direction. These observations are intuitively in agreement with the rod-like morphology of the structure at normal incidence, with the short-wavelength transverse mode of the rods matching that of 10 nm Au nanoparticles (520 nm) and the long-wavelength longitudinal mode produced by the optical field along the rod-like structure.

To probe the gyrotropic behavior of this metamaterial, transmission measurements on the same twinned domains as above were taken with left- and right-hand circularly polarized light. The sample was tilted by 35° and rotated around the [110] surface normal. For each full turn there are two rotation angles for which the optical axis coincides with the chiral [111] direction of the gyroid, that is, the microscope "looks down" the unobstructed gyroid channels (inset in **Figure 5**, Supporting Information Movie S2). Figure 5 plots the normalized difference in gyrotropic transmission ΔT between right- and left-hand polarized light as a function of sample rotation angle, averaged over frequency region between 600 and 750 nm, where there is little spectral variation. The transmission of circularly polarized light is maximal for the two rotation angles (0° and 180°) where the optical axis is colinear with the [111] and [11-1] directions. By varying the rotation angle, the optical path is increasingly obstructed by Au struts, reducing $|\Delta T|$. The rotation of the sample therefore leads to the clear observation of chirality in this gyroid metamaterial. The gyrotropic transmission is again very well reproduced by a finite difference time domain calculation.

We have thus successfully created the first self-assembled chiral optical metamaterial with 3D structure. This material is continuous, has features on the 10-nm length scale and exhibits orientation-dependent color under linearly polarized incident light, as well as optical chirality. These findings pave the way for the potential mass production of optical metamaterials, which can lead to a variety of large-scale applications.

Experimental Section

Sample Preparation: The samples were prepared by using a triblock ISO copolymer to create several-micrometer-thick ordered films, which were slowly dried at room temperature. A detailed characterization of the ISO block copolymer used in this study confirms the formation of the chiral alternating gyroid morphology in the isoprene phase.[20] The isoprene block was then removed by UV etching, and the resulting network of pores was back-filled with gold by electrodeposition from the conducting substrate, up to a thickness that could be varied between 200 and 1000 nm. The remaining polymer was subsequently removed by plasma etching.

Optical Characterization: Confocal optical microscopy was performed using a 50-μm core optical fiber that served as a pinhole in the conjugate to the focal plane of a ×10 long working distance microscope objective, which allowed for collection of a signal with a spatial resolution below the sample domain dimensions. A broadband

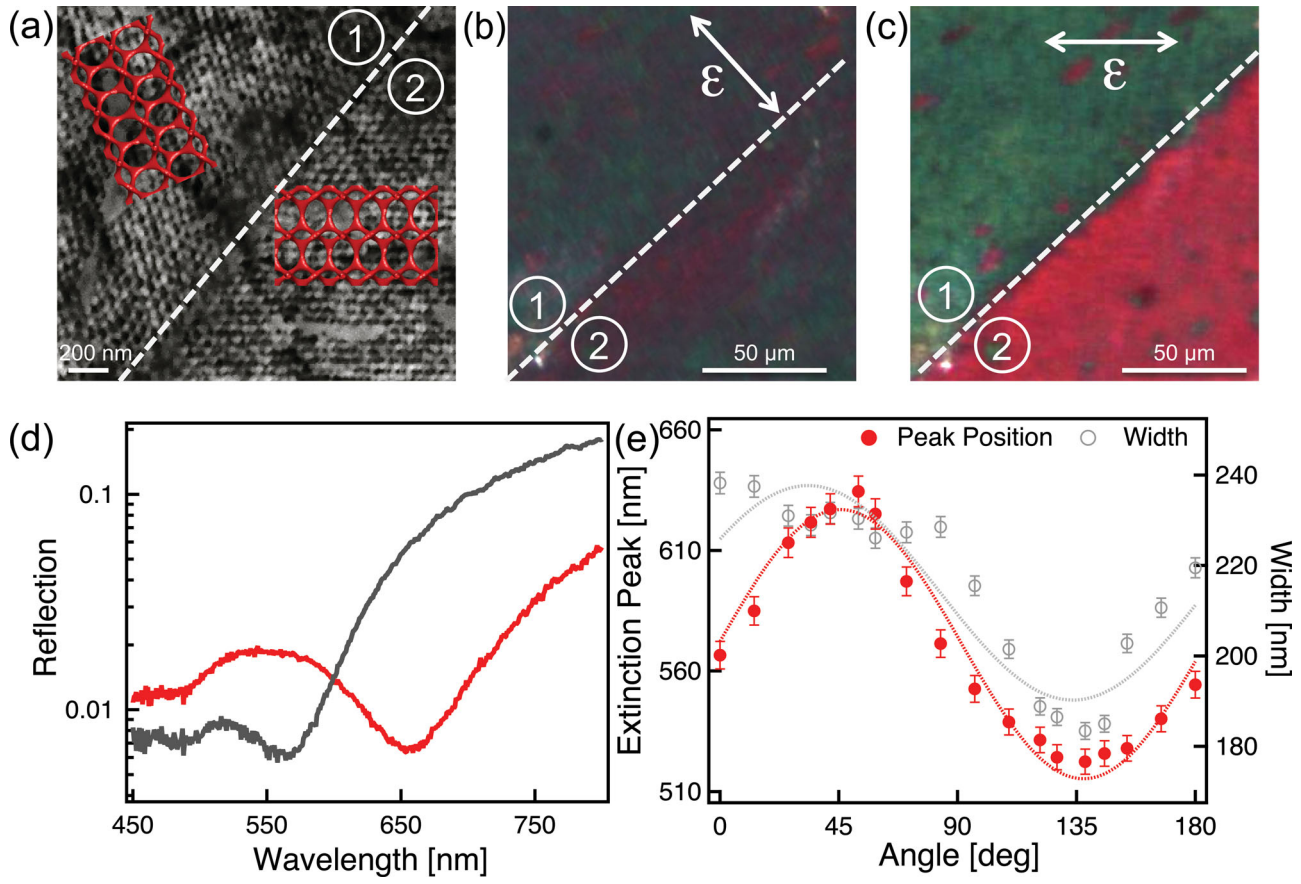

Figure 4. Linear dichroism of the Au gyroid. a) SEM image of the area where the optical measurements were performed. b,c) Optical reflection images obtained with linearly polarized illumination, indicated by white arrows. No optical contrast is observed for a polarization perpendicular to the grain boundary (b), while a polarization parallel to the gyroid [100] direction of one of the domains produces the largest optical contrast (c). d) Reflection spectra for Area 1 with incident polarization directions perpendicular (red) and parallel (grey) to the [100] gyroid direction. e) Variation in extinction (1−reflectivity) peak position and width as a function of the angle between [100] gyroid direction and incident light polarization.

halogen lamp acted as the illumination source. Linear polarization measurements were obtained using achromatic polarizers (Thorlabs, Inc.) and for circular polarization measurements the polarizers were combined with superachromatic quarter wave quartz plates (B. Halle Nachfl. GmbH). The sample was mounted on a multirotational stage that allowed rotation around the focal axis of the objective and tilting away from normal incidence. This configuration enabled transmission and reflection measurements to be taken in different directions of the sample, including chiral gyroid directions.

Theoretical Modeling: Self-consistent field theory was utilized to simulate a realistic triblock copolymer alternating gyroid morphology. The morphology of ISO was calculated, with relative block volume fractions of 0.28, 0.57, and 0.15 of I, S and O, respectively, using the simulation parameters previously reported[24] and the I domain was extracted for the finite-difference time-domain simulations. Transmittance, reflectance, and absorption of a 495 nm thick alternating gyroid film were simulated using a finite-difference time-domain simulator.[22] The material parameters previously reported for gold[23] were used.

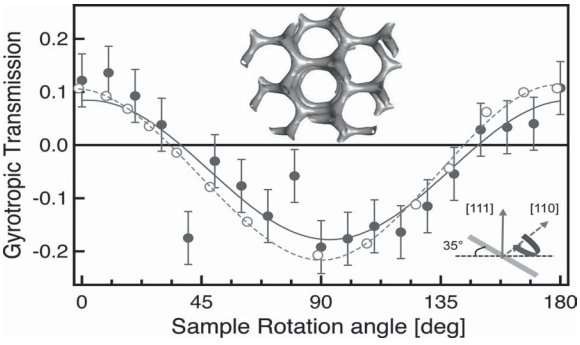

Figure 5. Gyrotropic transmission through a sample inclined at 35°. The gyrotropic transmission is the difference between the transmission spectra in left and right channels as the sample was rotated around the [110] axis. The open symbols are the results of a finite difference time domain calculation, while the full ones are the measurements. Lines are guides for the eye.

Supporting Information

Supporting Information is available from the Wiley Online Library or from the author.

Acknowledgements

S.V. and N.A.Y. contributed equally contribute to this work. The authors thank J. J. Rickard, M. Scherer and A. Finnemore for their invaluable help.

This publication was based on work supported in part by Award No. KUS-C1-018-02, made by King Abdullah University of Science and Technology (KAUST), the EPSRC grant EP/G060649/1 and by the National Science Foundation through the Materials World Network grant between the US (DMR-1008123) and the EPSRC.

Received: September 20, 2011
Published online:

[1] V. G. Veselago, *Sov. Phys. Uspekhi* **1968**, *10*, 509.
[2] J. B. Pendry, A. J. Holden, W. J. Stewart, I. Youngs, *Phys. Rev. Lett.* **1996**, *76*, 4773.
[3] J. B. Pendry, A. Holden, D. Robbins, W. Stewart, *IEEE Trans. Microwave Theory Tech.* **1999**, *47*, 2075.
[4] J. B. Pendry, *Phys. Rev. Lett.* **2000**, *85*, 3966.
[5] J. B. Pendry, D. Schurig, D. R. Smith, *Science* **2006**, *312*, 1780.
[6] U. Leonhardt, *Science* **2006**, *312*, 1777.
[7] D. R. Smith, W. J. Padilla, D. C. Vier, S. C. Nemat-Nasser, S. Schultz, *Phys. Rev. Lett.* **2000**, *84*, 4184.
[8] S. Xiao, V. P. Drachev, A. V. Kildishev, X. Ni, U. K. Chettiar, H.-K. Yuan, V. M. Shalaev, *Nature* **2010**, *466*, 735.
[9] E. Plum, V. A. Fedotov, A. S. Schwanecke, N. I. Zheludev, Y. Chen, *Appl. Phys. Lett.* **2007**, *90*, 223113.
[10] A. W. Clark, A. Glidle, D. R. S. Cumming, J. M. Cooper, *J. Am. Chem. Soc.* **2009**, *131*, 17615.
[11] M. Decker, M. Ruther, C. E. Kriegler, J. Zhou, C. M. Soukoulis, S. Linden, M. Wegener, *Opt. Lett.* **2009**, *34*, 2501.
[12] D. O. Güney, T. Koschny, C. M. Soukoulis, *Opt. Express* **2010**, *18*, 12348.
[13] M. Decker, M. W. Klein, M. Wegener, S. Linden, *Opt. Lett.* **2007**, *32*, 856.
[14] K. Lodewijks, N. Verelle, W. Van Roy, G. Borghs, P. Van Dorpe, *Appl. Phys. Lett.* **2011**, *98*, 091101.
[15] A. C. Edrington, A. M. Urbas, P. DeRege, C. X. Chen, T. M. Swager, N. Hadjichristidis, M. Xenidou, L. J. Fetters, J. D. Joannopoulos, Y. Fink, E. L. Thomas, *Adv. Mater.* **2001**, *13*, 421.
[16] I. Vukovic, S. Punzhin, Z. Vukovic, P. Onck, J. M. De Hosson, G. Brinke, K. Loos, *ACS Nano* **2011**, *5*, 6339.
[17] F. S. Bates, G. H. Fredrickson, *Phys. Today* **1999**, *52*, 32.
[18] T. H. Epps, E. W. Cochran, T. S. Bailey, R. S. Waletzko, C. M. Hardy, F. S. Bate, *Macromolecules* **2004**, *37*, 8325.
[19] W.-H. Tseng, C.-K. Chen, Y.-W. Chiang, R.-M. Ho, S. Akasaka, H. Hasegawet, *Nano Lett.* **2010**, *10*, 4994.
[20] M. Stefik, S. Wang, R. Hovden, H. Sai, M. W. Tate, D. A. Muller, U. Steiner, S. M. Gruner, U. Wiesner, unpublished.
[21] T. Bailey, H. Pham, F. S. Bates, *Macromolecules* **2001**, *34*, 6994.
[22] A. F. Oskooi, D. Roundy, M. i. Ibanescu, P. Bermel, J. annopoulos, S. G. Johnson *Comput. Phys. Commun.* **2010**, *181*, 687.
[23] A. Vial, A. S. Grimault, D. Macías, D. Barchiesi, M. L. de la Chapelle, *Phys. Rev. B* **2005**, *71*, 085416.
[24] C. A. Tyler, J. Qin, F. S. Bates, D. C. Morse, *Macromolecules* **2007**, *40*, 4654.